(TBME-01336-2017)

Cellular Obstruction Clearance in Proximal Ventricular Catheters Using Low-voltage Joule Heating

Abhay Sane, Kevin Tangen, David Frim, Meenesh R. Singh, and Andreas Linninger*

Abstract*— Objective: Proximal obstruction due to cellular material is a major cause of shunt failure in hydrocephalus management. The standard approach to treat such cases involves surgical intervention which unfortunately is accompanied by inherent surgical risks and a likelihood of future malfunction. We report a prototype design of a proximal ventricular catheter capable of non-invasively clearing cellular obstruction. Methods: In-vitro cell-culture methods show that low-intensity AC signals successfully destroyed a cellular layer in a localized manner by means of Joule heating induced hyperthermia. A detailed electrochemical model for determining the temperature distribution and ionic current density for an implanted ventricular catheter support our experimental observations. Results: In-vitro experiments with cells cultured in a plate as well as cells seeded in mock ventricular catheters demonstrated that localized heating between 43˚C to 48˚C caused cell death. This temperatures range is consistent with hyperthermia. The electrochemical model verified that Joule heating due to ionic motion is the primary contributor to heat generation. Conclusion: Hyperthermia induced by Joule heating can clear cellular material in a localized manner. This approach is feasible to design a non-invasive self-clearing ventricular catheter system. Significance: A shunt system capable of clearing cellular obstruction could significantly reduce the need for future surgical interventions, lower the cost of disease management and improve the quality of life for patients suffering from hydrocephalus.

***Index Terms*—Hydrocephalus, proximal obstruction, shunt revision, hyperthermia**

I. Introduction

IN SPITE OF the various complications that plague chronically implanted ventricular catheters [1],[2] ventricular CSF shunting remains the primary approach for hydrocephalus management [3]. However, shunt failure incidence after 1 year has been reported to be as high as 40 – 50% [4],[5] and long term studies show that multiple shunt revisions per patient are common [5]–[7]. A patient who experiences shunt failure is more likely to require repeated shunt revisions in the future [8],[9]. Proximal ventricular catheter occlusion, schematically represented in Fig. 1B, is a significant complication that causes shunt failure leading to a revision according to multiple clinical studies[5], [10]–[12]. An obstructed ventricular catheter fails to adequately drain CSF from the ventricles which causes the recurrence of hydrocephalus symptoms.

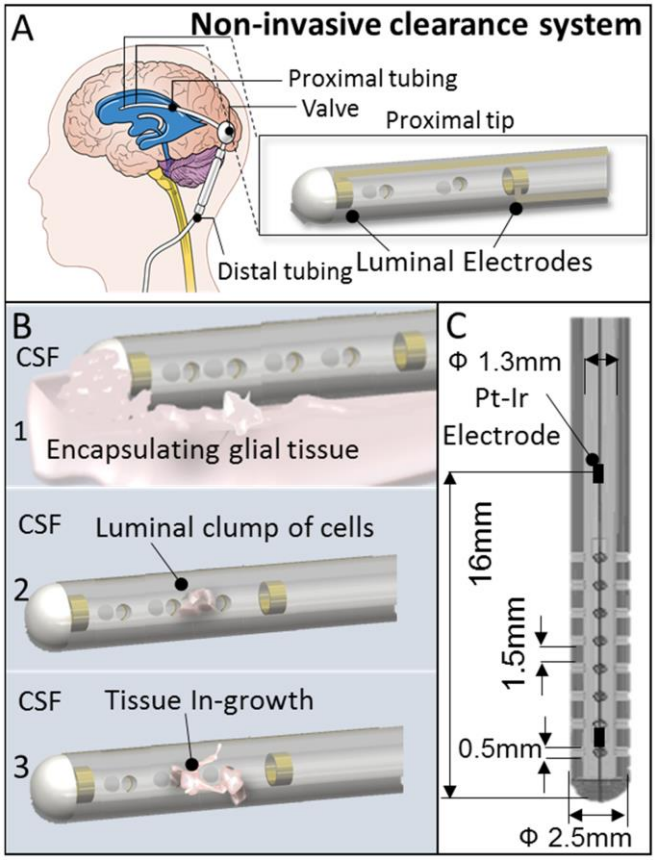

Fig. 1. Proposed non-invasive self-clearing proximal ventricular catheter. (A) Proposed design of ventricular catheter with luminal electrodes to induce hyperthermia by Joule heating. (B) Common varieties of ventricular catheter obstruction by (1) Glial encapsulation, (2) Luminal aggregate of cells and (3) Invasion of tissue via drain holes. (C) Geometry of modeled catheter, specifications taken from a commercially available catheter. It contains 4 rows of 8 drain ports that are cylindrical with a diameter of 0.5mm, all present within 16mm from catheter tip. The inter-port distance is 1.5 mm. Pt-Ir electrodes (black rectangles) are positioned close to the ports at the tip and beyond the distal ports to influence all common obstruction sites.

Currently, shunt revision is the standard operative approach to this complication. Several technological modifications to catheters have been introduced to reduce or prevent proximal obstruction in shunts [13]–[17]. Unfortunately, none of the innovations have significantly reduced proximal catheter

Partial support through an Innovator Award (P.I. A. Linninger) by the Hydrocephalus Association (directed by Dr. J. Koschnitzky) and NSF Grant # 1706921 is gratefully acknowledged.

Abhay Sane, Kevin Tangen and Andreas Linninger* are with the Department of Bioengineering, University of Illinois at Chicago, Chicago, IL 60607, USA. (email: linninge@uic.edu). Meenesh R. Singh is with the Department of Chemical Engineering at University of Illinois at Chicago. David Frim is with the Department of Neurology, University of Chicago, Chicago, IL 60637, USA. *Asterisk indicates corresponding author.*

occlusion. Methods such as electrocauterization [18]–[20] and ultrasound cavitation [21] have been used to reopen obstructed catheters, but both require surgical intervention and its attendant risks. Surgical shunt revisions are a burden to patients and the healthcare system [22],[23] and are a major source of morbidity associated with hydrocephalus. A shunt system that is capable of clearing obstructions internally and re-establishing CSF flow non-invasively without harming adjacent brain tissue would be of tremendous benefit for surgeons and patients. The use of microelectromechanical system (MEMS) based magnetic microactuators by Lee et. al. [24] to mechanically clear obstructing material is an example of progress in this direction.

. Hyperthermia involves raising and maintaining the temperature of a tissue, typically up to 43°C – 48°C, in order to destroy pathological cells. It is currently used as an adjunct therapy for treating tumors [25]. Although tumor tissue is more sensitive to hyperthermia, healthy tissue of the central nervous system is also susceptible to thermal injury [26]–[28] as are other cell types [29]–[31]. These studies indicate that hyperthermia can be an effective tool in clearing cellular obstruction in ventricular catheters. To address the pressing need for non-invasive clearance of catheter obstruction, we propose a design for a self-clearing ventricular catheter which induces **hyperthermia** by localized **Joule heating** that disintegrates obstructing cellular material and debris, and thus restores catheter patency. Joule heating is the process where the passage of an electric current through a conductor produces heat and is one mechanism of RF-induced heating. Applying an alternating electrical signal in the range of 10 kHz to 1 MHz in an ionic medium forces the ions in the medium to oscillate under the influence of the rapidly oscillating electric field. In this signal frequency range, the friction between the ions and solvent fluid (generally water) and the electrochemical reactions at the electrodes generates heat. The heating is proportional to the local current density which is highest near the electrode surface. Further away from the electrodes, the current density becomes smaller so that these regions are heated mainly by conduction of heat generated near the electrodes.

When the electrical signal frequency is in the GHz range, the dielectric properties of the medium become more prominent. Polar species, such as water molecules in a biological medium absorb energy from an incident EM signal, and oscillate or vibrate about their position, increasing their kinetic energy and generating heat. In this regime, the effect is known as *dielectric or capacitive heating* [32]. Because our signal frequency is below the range required for dielectric material properties to generate heat, we assume only Joule heating in the bulk, with dielectric heating confined to the electrical double layer at the electrode surface. We also expect *reactive heating* to occur at the electrode surface because of electrochemical reactions in response to the applied signal.

Based on these concepts, we propose a technique that can be adopted to clear obstructions in a hydrocephalus shunt to design a self-clearing ventricular catheter, shown in Fig. 1A as a schematic. Hyperthermia can be induced by means of low-voltage Joule heating using a set of electrodes in the proximal catheter lumen with wires embedded within the length of the catheter walls. Low-amplitude alternating voltage (**12V**) applied to the luminal electrodes to generate alternating currents (at **522.6 kHz**, similar to signal frequencies used clinically in radiofrequency tumor ablation) will generate heat that can disintegrate the obstructing material near the electrodes and reestablish CSF flow. This design is not unlike the system proposed in [33]. However, a significant difference is the use of *low-intensity electrical signals* (10 to 12V compared to 1000V for Non-Thermal Irreversible Electroporation (NTIRE) [34] or 30V for Radiofrequency ablation [35]) to induce hyperthermia, instead of tissue ablation. The proposed temperature window to be maintained ranges from 43°C–48°C. This modest temperature rise also contrasts with radiofrequency ablation and lesioning which near instantaneously destroys tissue by heating it to temperatures in excess of 60°C and often reach up to 100°C. Additionally, our design adopts lower intensity electrical signals, induces highly localized effects and lower temperatures and we will demonstrate that a well-designed shunt can localize the temperature distribution and prevent damage to neighboring cerebral structures.

In this original research paper, we show that a monolayer of C6 glioma cells seeded in a silicone tube lumen can be killed in a localized region by Joule heating. The heating method destroys cells seeded in the lumen of the mock ventricular catheter, while at the same time not visibly affecting cells present outside the catheter. In practice, the method aims at preventing injury to brain tissue lining a lateral ventricular cavity that is present near an implanted catheter. These proposed modifications to ventricular catheter design could provide a solution to the search for a non-invasive approach to clearing catheter obstructions.

II. Materials and Methods

The extent of cell death due to low-voltage Joule heating was first tested on cells cultured in a plate. Then, the method was tested on cells seeded in a silicone catheter lumen to determine whether the cellular destruction zone could be localized to the ports and lumen of the catheter. The temperature was measured using thermistors inside and outside the catheter. Finally, to validate our experimental observations, a 2D axisymmetric model of a ventricular catheter with luminal electrodes was created. The ionic current distribution over 1 cycle of the signal was determined and used to predict a steady-state temperature rise in the catheter lumen and surrounding ventricular space. Finally, the spatial distribution of temperature, current density and the potential gradient were analyzed to assess the risk of injury to the surrounding cerebral tissue layer.

A. Effect of Low-Voltage Joule Heating on C6 Glioma Cells in Culture.

The effect of low-voltage Joule heating was tested on C6 glioma cells in culture. Glial cells are major contributors to catheter obstruction [36], [37] and this cell line was chosen for its resilience and rapid growth rate. A schematic of the experimental setup is shown in Fig. 2A. The cells were maintained in Dubelcco's Modified Eagle's Medium (DMEM) fortified with 10% fetal bovine serum (FBS) (Gibco) in a CO_2 incubator (Steri-Cycle i160, Thermo Scientific) and a monolayer was grown in a 35 mm cell culture plate. A Wein

bridge oscillator circuit was assembled using discrete components on a printed circuit board (PCB) as the source of the clearance signal. The circuit was powered by a DC voltage source using a pack of Li-ion batteries (Sparkfun Electronics). The generated sinusoidal output signal (522.6 kHz, ±7V, Fig. 2A inset) was verified with an oscilloscope (Tektronix TDS 210). Stainless steel electrodes (O.D. 0.5144 mm) were mounted in a circular configuration to the dish cover.

The entire assembly was incubated at 37°C in the CO_2 incubator and the cells were exposed to the alternating signal for a period of 2, 4, 8 and 24 hours. After the experiment, the electrodes and electronics assembly were removed from the plate. Cell survival was analyzed using the tetrazolium dye MTT (Sigma Life Sciences) based viability assay. Live cells stained purple, while a clear colorless zone indicated the region of cell death. The size of the clearance zone was measured by integrating the area occupied by the zone using a standard grid of size 0.25mm^2. To test our hypothesis that the cell death was due to low-voltage Joule heating alone, the cell culture plate was placed in a water bath that acted as a heat sink. The clearance signal was applied for 24 hours with the heat sink and the area of the clearance zone was compared to that in cell culture plates treated in the absence of any thermal control.

B. Localization of Cell Death Following Low-Voltage Joule Heating Inside a Ventricular Catheter Lumen

Mock proximal ventricular catheters were fabricated in-house according to commercial dimensions using medical grade silicone tube (O.D. 0.125", I.D. 0.063"). The tube was cut into pieces of length 3cm and 2 rows of 7 ports (inter-port distance 3-4 mm) were punched using a 0.5mm steel needle punch to represent drain holes. Platinum-Iridium (Pt-Ir) ring electrodes (A-M Systems, WA; length 3.6mm, O.D. 1.4mm) were inserted into the lumen and positioned 7.5 mm apart in the center of the catheter. An insulation coated Pt-Ir wire (A-M Systems, WA; O.D. 0.008" coated) was spot welded to each electrode and the leads extended through the catheter wall and connected to the signal generator. C6 cells suspended in DMEM medium (approx. 10^6/ml) were loaded inside the catheter lumen and the mock shunt was submerged in fresh DMEM medium and incubated at 37°C for 3 days. The mock self-clearing ventricular shunt was suspended above a cell monolayer in another 35mm plate such that the shunt was at a distance of approximately 5mm from the external cell layer. The low-voltage signal (522.6 kHz, ±12V) was applied to the luminal electrodes in the experimental shunts for a period of 24 hours. After the specified experiment duration, the suspended shunts were removed and placed inside cell culture medium in a separate plate. An MTT viability assay was performed on cells inside the catheter lumen and separately, on cells external to the catheter in the cell culture plate. Control shunts were prepared in a similar fashion, except that no signal was applied to the luminal electrodes.

C. Temperature Measurements

The temperature rise due to Joule heating in the medium on application of the signal was measured to determine the extent of heating in the plate and the mock ventricular catheter. A thermistor (NTC 10kΩ, Amphenol) was suspended in the cell culture medium and the temperature measured in the plate at 2 locations – (i) near the ground electrode where the alternating current would be focused (due to the electrode configuration) and (ii) outside the circle formed by the peripheral electrodes. To obtain the temperature measurements, a multimeter (Elenco M-1750) in resistance measurement mode was used (source current approx. 17 μA at 10kΩ). The resistance was converted to the measured temperature using the Steinhart's equation (1), with the relevant coefficients obtained from the thermistor's specification sheet.

$$\frac{1}{T} = \mathrm{A} + \mathrm{B}\cdot\frac{\ln R}{R_0} + \mathrm{C}\cdot\left(\frac{\ln R}{R_0}\right)^2 + \mathrm{D}\cdot\left(\frac{\ln R}{R_o}\right)^3 \quad (1)$$

where T is the temperature in Kelvin, R is the measured resistance at temperature T, R_0 is the nominal resistance at ambient temperature (10kΩ at 25°C), and coefficients A, B, C and D are obtained from the product specification sheet (A=3.354E-03, B=2.562E-04, C=2.082E-06, D=7.300E-07). Measurements were also performed for experiments with proximal ventricular catheter tips suspended in the cell culture medium. The thermistors were placed inside the catheter lumen and in the medium external to the catheter.

D. Electrochemical Modeling of Proximal Ventricular Catheter

Ionic currents and thermal simulations were performed in COMSOL Multiphysics v5.2 (Burlington, MA) to predict the temperature elevation induced by electrical heating in an implanted silicone proximal ventricular catheter and the surrounding ventricular space. The catheter (Fig. 1C) was modeled on commercially available ventricular catheters (I.D. 1.3mm, O.D. 2.5mm, 4 rows of 8 port holes) [38]. Relevant thermal properties of CSF and silicone were taken from literature [39] and COMSOL's material library respectively, tabulated in the Online Supplementary Material, Table III. Electrodes were positioned around the port area corresponding to our experiments. Lateral ventricle geometry was simplified as an ellipsoidal volume. We considered 2 cases: a normal ventricle (volume = 20.9ml) as shown in Fig. 4A1 and a slit ventricle (volume = 1.15ml) shown in Fig. 4B1. In both cases, we have assumed that the catheter is optimally placed in the center of the ventricle, equidistant from the ventricular walls, and a layer of cerebral tissue (5 mm thick) was modeled to predict the thermal energy penetrating into the tissue. To reduce computational time, we took advantage of the axial symmetry of our model and performed the simulation on a single 2D slice. The 2D slice, divided using an unstructured triangular mesh, was composed of 108,144 elements for the normal ventricle and 96,400 for the slit ventricle.

Our model accounts for electrochemical reactions and concentration polarization that occur in case of an externally applied potential to an electrochemical system, and are often neglected in a simple electrical model. A transient simulation was performed over 1 cycle (2μs) of our signal (500 kHz) to determine the ionic flux, current density and potential distribution in CSF in response to the changing potential at the electrodes. The time-averaged current density obtained from the electrochemical cell model was used in the bulk heat-source

term (Q_{bulk}), whereas the time-averaged kinetic overpotential at the electrode surface and capacitive heat dissipation was used in the boundary heat-source terms ($q_{S,rxn}$ and $q_{S,cap}$) of the heat-transfer equation to predict temperature rise in the CSF and tissue regions of our model. The electrochemical system adopted for our model is explained in the Online Supplementary Material. Briefly, water molecules undergo electrolysis at the electrode surfaces in response to the applied AC signal. The time-averaged electrical current densities and overpotentials were used to calculate the heat generated in our model and then used to solve a steady-state heat transfer equation without flow representing a non-draining ventricular catheter in Eqn. (5).

$$0 = \vec{\nabla} \cdot \left[k\vec{\nabla}T(\vec{x})\right] + Q_{bulk} + Q_t \quad (5)$$

Here, $T(\vec{x})$ is the temperature at position $\vec{x}$, k is the thermal conductivity and Q_{bulk} is the heat generated in the bulk CSF and Q_t is the heat removed by capillary blood perfusion in the tissue layer.

1) Heat Source in CSF: The energy added to the domain by Joule heating in the bulk electrolyte is given by

$$Q_{bulk} = \vec{\nabla}V(\vec{x}) \cdot \sum_i \left(z_i F \vec{J}_i\right) \quad (6)$$

Q_{bulk} is the heat generated per unit volume (Wm^{-3}), $\vec{J}_i$ is the flux in the CSF ($molm^{-2}s^{-1}$) and z_i is the charge number of ionic species *i*, F is Faraday's constant ($Cmol^{-1}$) and $V(\vec{x})$ is the potential field in CSF (Vm^{-1}).

2) Heat sources in the tissue: Brain tissues have a dense capillary network and we assume the perfusing blood to behave as an infinite sink that remains at constant temperature [40], [41]. Q_t (Wm^{-3}) represents heat withdrawn by capillary blood perfusion in the tissue layer given in Eqn. (7)

$$Q_t = -\rho_b w_t C_{p_b}[T(\vec{x}) - T_b] \quad (7)$$

where ρ_b is the density of blood (kgm^{-3}), w_t is the volumetric blood perfusion rate in the tissue per unit volume ($mlcm^{-3}s^{-1}$), (in this case for the brain), Cp_b is the specific heat capacity of blood ($Jkg^{-1}K^{-1}$) and T_b is the temperature of the blood. The negative sign indicates heat is withdrawn by capillary perfusion. Metabolic heat generated in the tissue is neglected.

3) Electrochemical Initial and Boundary Conditions: The initial field potential at all positions in the model was set to 0V.

$$V(\vec{x}) = 0 \quad (8)$$

A current distribution initialization step was implemented to enable convergence of the dynamic simulation. The inner surface, Ωi of the tissue layer surrounding the ventricular fluid space is modeled as an insulator with normal current density set to zero.

$$\left[\sum_i z_i F \vec{J}_i\right]|_{\Omega i} = 0 \quad (9)$$

The potential at the electrode proximal to the catheter tip is chosen to be the anode and a sinusoidal potential is applied on the electrode boundary, with the other electrode acting as the cathode and ground.

$$V_{anode} = V_0 \sin(2\pi f t) \text{ and } V_{cathode} = 0 \quad (10)$$

V_0 is the amplitude of the signal which is set to 10V and f is the signal frequency, set to 500kHz. The electrode assignment is reversed in the second half of the cycle.

4) Temperature Initial and Boundary Conditions: The CSF and tissue are initially assumed to be at core body temperature of 310.15K. The external tissue surface is assumed to be an insulating surface

$$\vec{q}|_{\Omega o} = 0 \quad (11)$$

where $\vec{q}|_{\Omega o}$ is the heat flux normal to the *outer surface* of the tissue layer surrounding the lateral ventricle. Since the temperature elevation was moderate (<10°C), the CSF parameters were assumed independent of temperature.

5) Heat Sources at the Electrodes: The electrode surfaces are modeled as boundary heat sources composed of electrochemical reactive and capacitive heating.

(a) Electrochemical Reactive Heating: This heat is generated because of the overpotential at the interface. A time-averaged value for the heat flux (Wm^{-2}) in a single cycle was used as the heat source, given by Eqn. (12)

$$q_{S,rxn} = \frac{\int_0^2 (i_{rxn} \cdot \eta) dt}{2} \quad (12)$$

Where i_{rxn} is the current density at the interface due to the reaction (Am^{-2}), and η is the overpotential at the electrode (V), and the integration step provides a time-averaged value over a cycle of 2μs.

(b) Capacitive Heating: This component of the boundary heat source is due to the capacitive nature of the double layer at the interface. The heat flux (Wm^{-2}) produced in a non-ideal dielectric of a capacitor [42] is given by

$$q_{S,cap} = V_{cap}^2 \cdot \omega \cdot C_{dl} \cdot DF \quad (13)$$

where V_{cap} is the RMS potential (V) across the interfacial double layer which is found to be 0.23V using the Debye-Huckel formulation [43], ω is the frequency of the applied signal, C_{dl} is the specific capacitance (Fm^{-2}) of the double layer and DF is the *dissipation factor* signifying energy dissipated as heat in the dielectric. For the double layer interface, the dielectric is assumed to be water, which has a DF of 0.05 [44].

III. Results

A. *Effect of low-voltage Joule heating on C6 glioma cell in culture.*

The region of cell death can be clearly seen as a circular zone round the central electrode. The extent of this zone was found to increase when the clearance signal was applied for longer durations. When the signal was applied for a 2hr period, the area was found to be 0.55±0.57mm^2 in a circular shape around the central electrode and 47.42±18.51mm^2 for 24 hours. The cleared area for different durations is listed in Table I. Representative experimental plates for each duration are shown for the various tested experiment durations in Fig 2B. Fig. 2C shows the variation in the area of dead cells (red circles) measured versus duration of the applied signal. The use of an external water bath around the cell culture plate as a heat sink

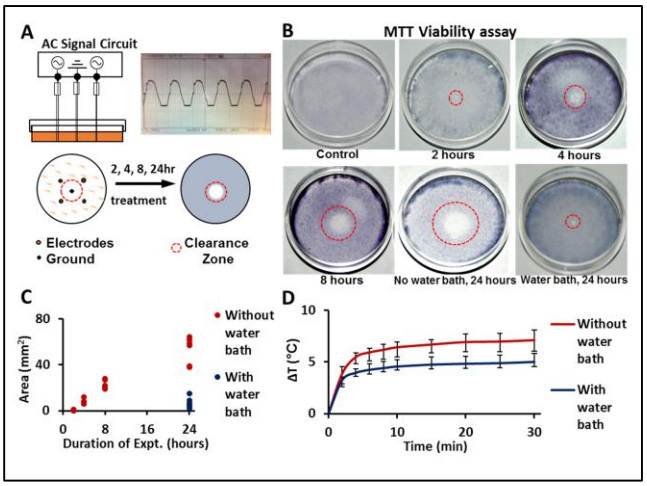

Fig 2: Low-voltage *Joule heating* induces cell death. (A) C6 Glioma monolayers cultured in 35 mm plates were exposed to a low-voltage AC signal to induce resistive heating in the medium. The generated waveform applied to the electrodes is shown in the inset. Experiments show that a circular configuration of electrodes successfully destroys cells to form a cell death zone (red circles) around the central electrode. (B) Representative images of experimental cell plates shown using an MTT viability assay performed after exposure to 0 (control), 2, 4, 8 and 24 hours of Joule heating, as well as one with a water bath to decrease temperature elevation. Keeping a water bath outside the cell plate during electrical treatment decreases the cell death area measured by the MTT viability assay. (C) The effect of exposure durations on cell death area. Blue circles indicate the presence of a water bath to control temperature elevation (D) Temperature measurements verified heating as the cause of cell death. A smaller temperature rise was observed due to the presence of the water bath which acted as a heat sink. The measurements were performed under ambient conditions in DMEM medium using a thermistor placed close to the central ground electrode (coinciding with the observed region of cell death).

reduces the region of cell death. The average area of the cell death by the applied signal for a duration of 24 hours was found to be 2.68±1.9mm^2 with a heat sink in place and the maximum area was found to be 5.5 mm^2 as compared to an average area of 47.42±18.51mm^2 without the water bath (Fig 2C, blue circles). We measured the temperature at the central electrode that corresponded to the region of cell death in the presence and absence of a water bath. The measurements showed that the external water bath reduced the extent of temperature elevation to an average of 5°C near the central electrode, as compared to 7.1°C without the external water bath (Fig 2D).

B. Localization of cell death following low-voltage Joule heating inside a ventricular catheter lumen.

The low-voltage Joule heating method applied to cells seeded in a ventricular catheter lumen is illustrated in the schematic of Fig. 3A. Samples of the mock proximal ventricular catheters seeded with C6 glioma cells exposed to Joule heating treatment are shown in Fig. 3B (top row) and control shunts with no treatment are shown in Fig. 3B (bottom row). The MTT assay elucidates a clear zone inside the catheter between the electrodes. The cells outside the catheter in the external cell culture plate stained purple after an MTT assay indicating their viability. Temperature measurements were carried out under ambient conditions in DMEM culture medium inside the catheter lumen. The temperature elevation is 7-8°C over 10min, depicted in Fig. 3C and remains steady till 24 hours. The temperature rise outside the catheter is 3-5°C and is insufficient to kill cells. The positions of the thermistors during temperature measurements are shown as white filled circles in Fig. 3A.

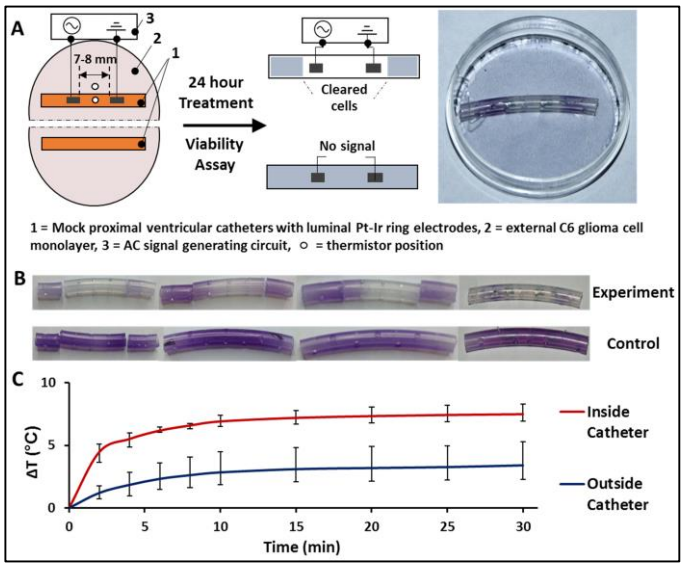

Fig 3: Localized effect of low-voltage Joule heating on a C6 cell monolayer in a mock proximal ventricular catheter. The schematic of the experimental setup is shown in (A). Cells in the region between the luminal electrodes inside the proximal ventricular catheter are killed, while the cell monolayer in the external plate are unaffected after performing the MTT viability assay (right) (B) Representative images of experimental (top) and control catheters (bottom). A clear zone is seen in the middle of the experimental catheters which corresponds to the region between and around the luminal electrodes (n = 6). (C) Temperature measurements inside and outside the catheter (marked by black circles in panel A) show that heating is significantly greater inside the catheter lumen.

C. Electrochemical modeling of a proximal ventricular catheter

An electrochemical analysis of hyperthermia in a proximal ventricular catheter was conducted to support our experimental observations. We calculated the peak ionic current density induced in the electrolyte for a single cycle of the applied signal and then predicted the spatial temperature distribution at steady state. The maximum temperature in CSF and the ventricular wall are of particular significance, as they indicate the volume influenced by our signal around the catheter and possible thermal damage to the ventricular wall respectively.

For a normal ventricle, the simulations predict that the temperature rise is confined to the region adjacent to the luminal electrodes, as shown in the axial slice in Fig 4A2. 2D heat maps from the planes X′-X″ near a luminal electrode and Y′-Y″ between the luminal electrodes are shown in Figs. 4A3 and 4A4 respectively. Predicted temperature distributions and current density distributions along centerlines Z′-Z″ of the heat maps are plotted adjacent to the heat maps. Elevated temperatures are clearly confined to inside the catheter lumen and around the ports – regions that are frequently obstructed. Inside the lumen, the temperature rise is predicted to a maximum of 50.9°C at the electrodes. In the CSF filled space outside the catheter wall, the temperature rises to a maximum of 48.6°C at a port adjacent to a luminal electrode and does not exceed 38°C at the ventricular

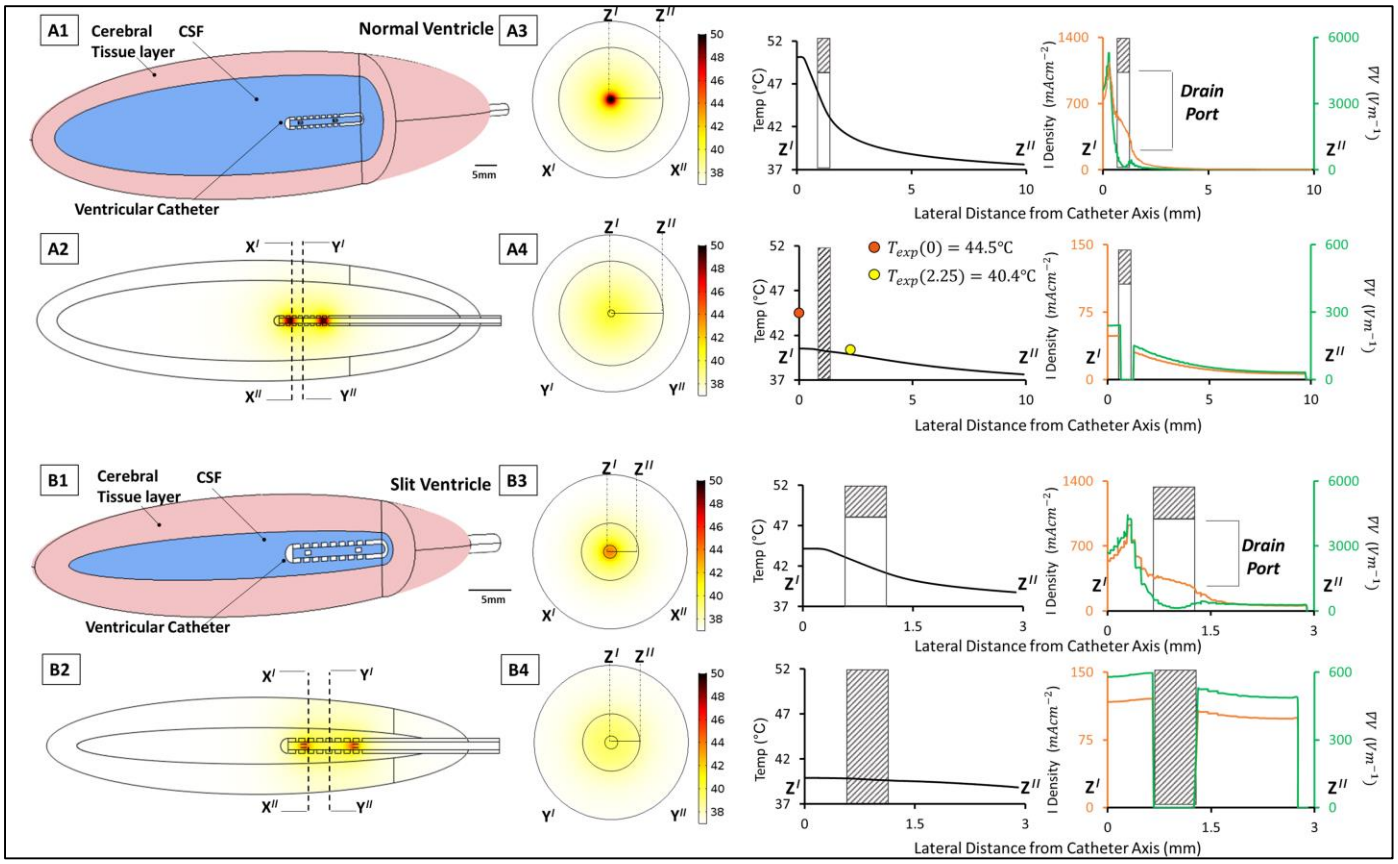

Fig 4: Computational model of the heating in an implanted ventricular catheter suspended in a CSF-filled normal ventricle (A1-A4) and slit ventricle (B1-B4). The lateral ventricle filled with CSF (blue domain) is surrounded by a 5mm layer of tissue (pink domain). An alternating electric signal of 10Vpeak and is applied to a luminal electrode, the other being ground. Panel A represents a "normal ventricle" with a maximum cross-sectional diameter of 10mm (Volume = 20.9 ml) and panel B represent the extreme case of a "slit ventricle" with a maximum cross-sectional diameter of 6mm (Volume = 1.15ml) Panels A2 and B2 show the heat map denoting the temperature distribution on the central cut-plane at steady state in the "normal ventricle" and slit ventricle respectively. Planes X′-X″ near the luminal electrode closer to the catheter proximal tip and Y′-Y″ between the luminal electrodes are marked in panels A1 and B1. 2D heat maps in these planes are shown in panels A3, A4, B3 and B4 Temperatures at steady state predicted by the simulations along the line Z′-Z″ are plotted in panels A3 and A4 for the "normal ventricle" and in panels B3 and B4 for the slit ventricle. The catheter wall is depicted as a grey dashed region, with the drain port found in plane X′-X″ depicted and labelled. Similarly, ionic current density (orange) and the gradient of electrolyte potential (green) at peak applied signal amplitude (0.5μs) is plotted along the same line Z′-Z″.

wall. The maximum current density inside the lumen is predicted to be 3320.7mAcm^{-2} at the electrode surface and 1428.3mAcm^{-2} in the CSF outside the catheter. The current drops to near zero (<10mAcm^{-2}) at the ventricular wall. We also compare the values of heat sources in the bulk as well as at the electrode surfaces to determine their relative contributions to hyperthermia. The heat generated because of the kinetic overpotential at the interface is 3.34×10^{-3}W, the capacitive heat dissipated in the interfacial double layer is 7.39×10^{-5}W and the heat dissipated in a 0.57mm^3 cylindrical envelope of CSF around an electrode is 2.27×10^{-2}W. From this comparison, we can conclude that Joule heating due to bulk ionic motion in is the most important contributor to the temperature elevation.

Our simulation for a slit ventricle (Fig 4B) predicts the temperature distribution for the tissue layers close to the electrodes. The temperature and current density distributions are shown in Fig 4B4 in the planes X′-X″ near a luminal electrode and Y′-Y″ between the two electrodes. Inside the lumen, the maximum temperature is predicted to be 44.8°C near the electrodes, 43.5°C at the port and attains a maximum of 39.2°C at the ventricular wall. The maximum current density inside the lumen is predicted to be 2327.2mAcm^{-2} at the electrode surface, 1063.9mAcm^{-2} in the CSF outside the port near each electrode.

IV. Discussion

Proximal ventricular catheter obstruction is the leading cause of shunt failure requiring risky shunt revision. Current clinical standards of care rely on costly shunt replacements or invasive clearance procedures. A non-invasive methodology to remove the obstruction and reestablish CSF flow could tremendously improve the quality of life for hydrocephalus patients by minimizing the need for surgical revisions and reducing morbidity as well as the cost of hydrocephalus management. Current methods to clear obstruction without shunt replacement, such as HIFU ablation and electrocautery, require an invasive surgical procedure to insert a probe into the ventricular catheter. Our aim was to design a self-clearing ventricular catheter system that utilized low-voltage Joule heating to clear cellular obstructions.

Using cell culture experiments, we demonstrate that cell death can be induced using low-voltage Joule heating. A rise in temperature near the central electrode corresponded to the

region of cell death. Temperature measurements at the central electrode indicate a maximum temperature rise of 8°C. In a biological environment at 37°C, this will result in a local temperature in the region of 43°C – 48°C which falls in the range of cell death by hyperthermia [25]. In experiments with mock ventricular shunts, we observed that the low-voltage signal applied to the luminal electrodes caused cell death only inside the lumen and spared the cells outside the catheter. These results show that low-voltage Joule heating to remove cellular obstruction in a proximal ventricular catheter and reestablish CSF flow is feasible. With regard to this finding, it would also be interesting to study whether a periodic heating regime could inhibit the growth of obstructing material and prevent proximal ventricular catheter obstruction in a *prophylactic* way. For this purpose, a follow-up study that investigates cell growth rates with periodic low-voltage Joule heating in a catheter test system as described in [45] would be very useful.

We developed an electrochemical model to elucidate heat generation and temperature profiles for a self-clearing proximal ventricular catheter. We modeled a catheter implanted in a normal ventricle and also implanted in the extreme case of a slit ventricle that posed the maximum potential for thermal injury to cerebral tissue surrounding the ventricular cavity. The simulations predicted a temperature rise at the lateral ventricular cell boundary of 0.6°C in the normal ventricle and 2.2°C in the slit ventricle. In both cases, the ventricular wall remains <40°C at steady state. These temperature levels at the boundary of the ventricle [26]–[28] are unlikely to damage the periventricular cell layer. Our preliminary simulations and in-vitro experiments indicate that the effect of low-voltage Joule heating is confined to the shunt lumen and the catheter ports. We perceive value in our model for the purpose of selecting appropriate electrical signal parameters based on the desired temperature distribution, catheter position and in predicting the risk of injury to the periventricular tissue.

An added benefit of using low-voltage Joule heating to induce *hyperthermia* is that the mechanism of cell death is typically apoptosis [46]–[48]. This offers a considerable advantage compared to aggressive thermal or mechanical strategies that largely induce necrotic cell death. Apoptotic cell death induces a minimal inflammatory response compared to necrotic cell death and reduces the likelihood of consequent cellular aggregation and scarring and thereby reducing the risk of repeated obstruction and shunt failure. The cellular mechanism of thermal injury to tissues surrounding the ventricle would require further experimental study. There is precedence in the use of thermal methods near ventricular tissues, such as choroid plexus cauterization, used previously in the management of certain etiologies of hydrocephalus [49]–[51] and the extraction of catheters adhering to the ventricular wall [52],[53]. Furthermore, a non-invasive method using capacitive RF energy transfer that has also been tested and proven to be effective in inducing hyperthermia in intracranial tumors could also be adopted [54],[55]. We also expect local pH changes at the electrodes because of the surface reactions. It is possible that these changes may also contribute to cell death, by mechanisms seen in electrochemical therapy [56] such as protein denaturation and cell permeabilization by extreme pH changes (<1 or >13) and the action of reactive byproducts of electrochemical processes. However, such conditions are usually observed in case of a sustained DC signal and as we have a rapidly changing AC signal, we do not expect these effects to be very significant.

We acknowledge several limitations in our study. Experiments and simulations were carried out without CSF flow, and therefore, do not account for the CSF drainage through a partially obstructed catheter or the pulsatile flow dynamics of CSF in the ventricular system [57]–[59]. Additionally, although we accounted for heat withdrawal by capillary perfusion, we insulated the outer surface of the model domain. These assumptions tend to overestimate the temperature rise and likelihood of thermal damage to tissue. CSF oscillations also lower the risk of damaging adjacent healthy tissue because the dynamic fluid disperses heat more efficiently by convection. In this situation, a higher intensity signal may be safely applied without the risk of periventricular tissue damage. An alternative solution would be to use different electrode configurations such as arrays of axial electrodes that may be designed to optimize the thermal dose in the commonly obstructed regions of the catheter, while minimizing risk to the adjacent ventricular tissue. Different configurations and power densities can be conveniently tested in an in-vitro setup using flow bioreactors as described by Harris et. al. [45] or Basati et. al. [60] to optimize ventricular catheter designs.

We have assumed ideal catheter placement in the center of a ventricle. In practice, catheters may be located, suboptimally, closer to lateral ventricular wall. Such scenarios will be explored in future work. However, the higher conductivity of CSF as compared to tissue (ratio 10:1) permits only a small fraction of the current to flow through brain tissue. Additionally, current density maps in Fig.4 show that local ionic current density is likely to be higher near the catheter and falls rapidly with distance away from the catheter. Our group has previously developed a catheter obstruction sensor [60] that could be integrated to detect the degree of luminal obstruction and use this information to modulate appropriate signal.

Another source of potential limitations concerns MR-induced heating due to an implanted wiring. Clinical cases in which patients with metallic implants suffer from moderate to severe burns during an MRI are well known. Since standard-of-care for hydrocephalus consists of frequent MRI scans, it is important to address the possible risks involved in the undesirable thermal response to our shunt design.

Two mechanisms nay cause undesirable heating in a metallic implant during an MRI scan [61]. Time-varying magnetic fields induce eddy currents in insulated metallic leads or metallic implants with large cross-sectional areas. Magnetic field influence on electrode leads is greater in coiled structures. We envision our electrode leads to be embedded within the silicone tube and do not utilize a coiled structure to minimize the risk of heating. Pt-Ir as an electrode material by itself has also been shown to be safe for deep brain stimulation and epilepsy monitoring during an MRI [62]–[64].

Secondly, catheter electrodes and leads may also act as antennas for the RF pulse sequences. The risk of RF interaction becomes higher in case of long wires due to resonance, when the wire length is an odd multiple of half-wavelength of the RF signal. The RF pulse signals in MRI are usually between 10 MHz to 100 MHz, from which the minimum length (half-wavelength) for resonant behavior is 7.5m – 1.5m. Our lead length will be below 100cm (approximate length to distal valve). Darcey et. al. [65] reported that the thermal effects of the antenna behavior were very low in short leads. Other design changes such as periodic air gaps [66] or "chokes" [67] in the leads change the impedance characteristics and decrease the resonance phenomena, also provide a means to reduce or eliminate resonance RF heating. Further guidelines for safe MRI for patients with metallic implants are discussed in [68].

V. Conclusion

Cellular obstruction of ventricular catheters is a significant cause of shunt failure necessitating shunt revisions. We propose a method to clear obstruction using Joule heating induced by an alternating potential applied to electrodes in the catheter lumen. Our in-vitro experiments indicate that the method has the potential to destroy cells in a localized manner inside the catheter lumen and ports, without harming cells outside the catheter. A detailed electrochemical model elucidates the different sources of heat generation and confirms that temperature elevations are sufficient to cause cell death in regions prone to obstruction and that temperature levels close to the ventricular wall are safe and unlikely to damage brain tissue. This study is a step towards developing a self-clearing ventricular catheter. In the future, we envision this work may contribute towards the development of a "smart shunt" which employs multiple systems in a feedback loop to both detect and non-invasively clear catheter obstruction.

VI. References

[1] S. R. Browd *et al.*, "Failure of Cerebrospinal Fluid Shunts: Part I: Obstruction and Mechanical Failure," *Pediatr. Neurol.*, vol. 34, no. 2, pp. 83–92, Feb., 2006a.

[2] S. R. Browd *et al.*, "Failure of Cerebrospinal Fluid Shunts: Part II: Overdrainage, Loculation, and Abdominal Complications," *Pediatr. Neurol.*, vol. 34, no. 3, pp. 171–176, Mar., 2006b.

[3] G. K. Reddy *et al.*, "Management of Adult Hydrocephalus with Ventriculoperitoneal Shunts: Long-term Single-Institution Experience," *Neurosurgery*, vol. 69, no. 4, Oct. 2011.

[4] J. Kestle *et al.*, "Long-term follow-up data from the Shunt Design Trial.," *Pediatr. Neurosurg.*, vol. 33, no. 5, pp. 230–236, Nov. 2000.

[5] J. Stone *et al.*, "Revision rate of pediatric ventriculoperitoneal shunts after 15 years," *J. Neurosurg. Pediatr.*, vol. 11, no. 1, pp. 15–19, Jan. 2013.

[6] S. Iglesias *et al.*, "Surgical outcome of the shunt: 15-year experience in a single institution," *Childs Nerv. Syst.*, vol. 32, no. 12, pp. 2377–2385, Dec. 2016.

[7] G. K. Reddy *et al.*, "Long-Term Outcomes of Ventriculoperitoneal Shunt Surgery in Patients with Hydrocephalus," *World Neurosurg.*, vol. 81, no. 2, pp. 404–410, Feb. 2014.

[8] J. A. Lazareff *et al.*, "Multiple shunt failures: an analysis of relevant factors.," *Childs Nerv. Syst. ChNS Off. J. Int. Soc. Pediatr. Neurosurg.*, vol. 14, no. 6, pp. 271–275, Jun. 1998.

[9] S. Tuli *et al.*, "Risk factors for repeated cerebrospinal shunt failures in pediatric patients with hydrocephalus," *J. Neurosurg.*, vol. 92, no. 1, pp. 31–38, Jan. 2000.

[10] B. M. Borgbjerg *et al.*, "Frequency and causes of shunt revisions in different cerebrospinal fluid shunt types," *Acta Neurochir. (Wien)*, vol. 136, no. 3, pp. 189–194, Sep. 1995.

[11] Patrick W. Hanlo *et al.*, "Treatment of hydrocephalus determined by the European Orbis Sigma Valve II survey: a multicenter prospective 5-year shunt survival study in children and adults in whom a flow-regulating shunt was used," *J. Neurosurg.*, vol. 99, no. 1, pp. 52–57, Jul. 2003.

[12] S. D. Ferguson *et al.*, "Observations regarding failure of cerebrospinal fluid shunts early after implantation," *Neurosurg. Focus*, vol. 22, no. 4, p. E7, Apr. 2007.

[13] K. R. Patel *et al.*, "Evaluation of polymer and self-assembled monolayer-coated silicone surfaces to reduce neural cell growth," *Biomaterials*, vol. 27, no. 8, pp. 1519–1526, Mar. 2006.

[14] A.-F. Gebert *et al.*, "Long-term survival rates of gravity-assisted, adjustable differential pressure valves in infants with hydrocephalus," *J. Neurosurg. Pediatr.*, vol. 17, no. 5, pp. 544–551, May 2016.

[15] R. W. Gruber and B. Roehrig, "Prevention of ventricular catheter obstruction and slit ventricle syndrome by the prophylactic use of the Integra antisiphon device in shunt therapy for pediatric hypertensive hydrocephalus: a 25-year follow-up study," *J. Neurosurg. Pediatr.*, vol. 5, no. 1, pp. 4–16, Jan. 2010.

[16] A. T. Villavicencio *et al.*, "Comparison of revision rates following endoscopically versus nonendoscopically placed ventricular shunt catheters," *Surg. Neurol.*, vol. 59, no. 5, pp. 375–379, May 2003.

[17] N. Jung and D. Kim, "Effect of Electromagnetic Navigated Ventriculoperitoneal Shunt Placement on Failure Rates," *J. Korean Neurosurg. Soc.*, vol. 53, no. 3, pp. 150–154, Mar. 2013.

[18] R. J. Hudgins and W. R. Boydston, "Shunt revision by coagulation with retention of the ventricular catheter," *Pediatr. Neurosurg.*, vol. 29, no. 2, pp. 57–59, Aug. 1998.

[19] J. V. Pattisapu *et al.*, "Percutaneous endoscopic recanalization of the catheter: a new technique of proximal shunt revision.," *Neurosurgery*, vol. 45, no. 6, pp. 1361-6; discussion 1366-1367, Dec. 1999.

[20] K. K. Gnanalingham *et al.*, "Percutaneous coagulation of choroid plexus to unblock the ventricular catheter using the Seldinger technique: preliminary report," *Surg. Neurol.*, vol. 64, no. 5, pp. 440–443, Nov. 2005.

[21] H. J. Ginsberg *et al.*, "Recanalization of obstructed cerebrospinal fluid ventricular catheters using ultrasonic cavitation," *Neurosurgery*, vol. 59, no. 4 Suppl 2, p. ONS403–412; discussion ONS412, Oct. 2006.

[22] T. Simon *et al.*, "Hospital care for children with hydrocephalus in the United States: utilization, charges, comorbidities, and deaths," *J. Neurosurg. Pediatr.*, vol. 1, no. 2, pp. 131–137, Feb. 2008.

[23] R. V. Patwardhan and A. Nanda, "Implanted ventricular shunts in the United States: the billion-dollar-a-year cost of hydrocephalus treatment," *Neurosurgery*, vol. 56, no. 1, pp. 139–145, Feb. 2005.

[24] S. A. Lee *et al.*, "Development of Microfabricated Magnetic Actuators for Removing Cellular Occlusion.," *J. Micromechanics Microengineering Struct. Devices Syst.*, vol. 21, no. 5, p. 54006, May 2011.

[25] M. Mallory *et al.*, "Therapeutic hyperthermia: The old, the new, and the upcoming," *Crit. Rev. Oncol. Hematol.*, vol. 97, pp. 56–64, Jan. 2016.

[26] P. Sminia *et al.*, "Effect of hyperthermia on the central nervous system: a review," *Int. J. Hyperth. Off. J. Eur. Soc. Hyperthermic Oncol. North Am. Hyperth. Group*, vol. 10, no. 1, pp. 1–30, Feb. 1994.

[27] S. Y. Lee *et al.*, "Acute histological effects of interstitial hyperthermia on normal rat brain," *Int. J. Hyperth. Off. J. Eur. Soc. Hyperthermic Oncol. North Am. Hyperth. Group*, vol. 16, no. 1, pp. 73–83, Feb. 2000.

[28] J. Haveman *et al.*, "Effects of hyperthermia on the central nervous system: what was learnt from animal studies?," *Int. J. Hyperth. Off. J. Eur. Soc. Hyperthermic Oncol. North Am. Hyperth. Group*, vol. 21, no. 5, pp. 473–487, Aug. 2005.

[29] V. R. Khan and I. R. Brown, "The effect of hyperthermia on the induction of cell death in brain, testis, and thymus of the adult and developing rat," *Cell Stress Chaperones*, vol. 7, no. 1, pp. 73–90, Jan. 2002.

[30] H. T. Belay and I. R. Brown, "Spatial analysis of cell death and Hsp70 induction in brain, thymus, and bone marrow of the hyperthermic rat," *Cell Stress Chaperones*, vol. 8, no. 4, pp. 395–404, Oct. 2003.

[31] P. S. Yarmolenko *et al.*, "Thresholds for thermal damage to normal tissues: An update," *Int. J. Hyperthermia*, vol. 27, no. 4, pp. 320–343, Jun. 2011.

[32] M. G. Lubner *et al.*, "Microwave Tumor Ablation: Mechanism of Action, Clinical Results and Devices," *J. Vasc. Interv. Radiol. JVIR*, vol. 21, no. 8 Suppl, pp. S192–S203, Aug. 2010.
[33] E. C. Ventureyra and M. J. Higgins, "A new ventricular catheter for the prevention and treatment of proximal obstruction in cerebrospinal fluid shunts," *Neurosurgery*, vol. 34, no. 5, pp. 924–926, May 1994.
[34] J. H. Rossmeisl Jr *et al.*, "Safety and feasibility of the NanoKnife system for irreversible electroporation ablative treatment of canine spontaneous intracranial gliomas," *J. Neurosurg.*, vol. 123, no. 4, pp. 1008–1025, Oct. 2015.
[35] Y. Miao *et al.*, "Evaluation of Radiofrequency Ablation as an Alternative for the Treatment of Brain Tumor in Rabbits," *J. Neurooncol.*, vol. 56, no. 2, pp. 119–126, Jan. 2002.
[36] C. A. Harris and J. P. 2nd McAllister, "What we should know about the cellular and tissue response causing catheter obstruction in the treatment of hydrocephalus.," *Neurosurgery*, vol. 70, no. 6, pp. 1589-601; discussion 1601-1602, Jun. 2012.
[37] B. W. Hanak *et al.*, "Toward a better understanding of the cellular basis for cerebrospinal fluid shunt obstruction: report on the construction of a bank of explanted hydrocephalus devices," *J. Neurosurg. Pediatr.*, vol. 18, no. 2, pp. 213–223, Aug. 2016.
[38] Medtronic, MN, "Medtronic Neurosurgery," 2017.
[39] D. A. Nelson and S. A. Nunneley, "Brain temperature and limits on transcranial cooling in humans: quantitative modeling results.," *Eur. J. Appl. Physiol.*, vol. 78, no. 4, pp. 353–359, Sep. 1998.
[40] E. J. Berjano, "Theoretical modeling for radiofrequency ablation: state-of-the-art and challenges for the future," *Biomed. Eng. OnLine*, vol. 5, no. 1, p. 24, Apr. 2006.
[41] M. M. Elwassif *et al.*, "Bio-heat transfer model of deep brain stimulation induced temperature changes," *Conf Proc IEEE Eng Med Biol Soc*, vol. 1, pp. 3580–3583, 2006.
[42] *The Electronics handbook*, Second ed. Boca Raton, FL: CRC Press, 2005.
[43] J. N. Israelachvili, "Electrostatic forces between Surfaces in Liquids," in *Intermolecular and Surface Forces*, Second., Academic Press, 1992, pp. 213–260.
[44] A. Von Hippel, "Water Loss tangent," in *Dielectric materials and applications*, MIT Press, 1954, pp. 361–362.
[45] C. A. Harris and J. P. McAllister, "Does drainage hole size influence adhesion on ventricular catheters?," *Childs Nerv. Syst.*, vol. 27, no. 8, pp. 1221–1232, Apr. 2011.
[46] P. Wust *et al.*, "Hyperthermia in combined treatment of cancer," *Lancet Oncol.*, vol. 3, no. 8, pp. 487–497, Aug. 2002.
[47] B. Hildebrandt *et al.*, "The cellular and molecular basis of hyperthermia," *Crit. Rev. Oncol. Hematol.*, vol. 43, no. 1, pp. 33–56, Jul. 2002.
[48] D.-C. Wang *et al.*, "Hyperthermia promotes apoptosis and suppresses invasion in C6 rat glioma cells.," *Asian Pac. J. Cancer Prev. APJCP*, vol. 13, no. 7, pp. 3239–3245, Jul. 2012.
[49] Benjamin C. Warf, "Comparison of endoscopic third ventriculostomy alone and combined with choroid plexus cauterization in infants younger than 1 year of age: a prospective study in 550 African children," *J. Neurosurg. Pediatr.*, vol. 103, no. 6, pp. 475–481, Dec. 2005.
[50] I. K. Pople and D. Ettles, "The role of endoscopic choroid plexus coagulation in the management of hydrocephalus," *Neurosurgery*, vol. 36, no. 4, pp. 698-701; discussion 701-702, Apr. 1995.
[51] Hideki Ogiwara *et al.*, "Obliteration of the choroid plexus after endoscopic coagulation," *J. Neurosurg. Pediatr.*, vol. 14, no. 3, pp. 230–233, Sep. 2014.
[52] P. Steinbok and D. D. Cochrane, "Removal of adherent ventricular catheter," *Pediatr. Neurosurg.*, vol. 18, no. 3, pp. 167–168, 1992.
[53] F. J. Martínez-Lage *et al.*, "Prevention of intraventricular hemorrhage during CSF shunt revisions by means of a flexible coagulating electrodeA preliminary report," *Childs Nerv. Syst.*, vol. 14, no. 4, pp. 203–206, Apr. 1998.
[54] R. Tanaka *et al.*, "Radiofrequency hyperthermia for malignant brain tumors: preliminary results of clinical trials," *Neurosurgery*, vol. 21, no. 4, pp. 478–483, Oct. 1987.
[55] G. Fiorentini *et al.*, "A Phase II Clinical Study on Relapsed Malignant Gliomas Treated with Electro-hyperthermia," *In Vivo*, vol. 20, no. 6, pp. 721–724, Nov. 2006.
[56] L. Jing-Hong and X. Yu Ling, "Electrochemical Therapy of Tumors," *Conf. Pap. Med.*, vol. 2013, p. 13, 2013.
[57] A. A. Linninger *et al.*, "Pulsatile cerebrospinal fluid dynamics in the human brain," *IEEE Trans. Biomed. Eng.*, vol. 52, no. 4, pp. 557–565, Apr. 2005.
[58] B. Sweetman *et al.*, "Three-dimensional computational prediction of cerebrospinal fluid flow in the human brain," *Comput. Biol. Med.*, vol. 41, no. 2, pp. 67–75, Feb. 2011.
[59] A. A. Linninger *et al.*, "Cerebrospinal Fluid Mechanics and Its Coupling to Cerebrovascular Dynamics," *Annu. Rev. Fluid Mech.*, vol. 48, no. 1, pp. 219–257, Jan. 2016.
[60] S. Basati *et al.*, "Impedance Changes Indicate Proximal Ventriculoperitoneal Shunt Obstruction In Vitro," *IEEE Trans. Biomed. Eng.*, vol. 62, no. 12, pp. 2787–2793, Dec. 2015.
[61] J. A. Nyenhuis *et al.*, "MRI and implanted medical devices: basic interactions with an emphasis on heating," *IEEE Trans. Device Mater. Reliab.*, vol. 5, no. 3, pp. 467–480, Sep. 2005.
[62] N. C. Bhavaraju *et al.*, "Electrical and thermal behavior of non-ferrous noble metal electrodes exposed to MRI fields," *Magn. Reson. Imaging*, vol. 20, no. 4, pp. 351–357, May 2002.
[63] J.-C. Georgi *et al.*, "Active deep brain stimulation during MRI: A feasibility study," *Magn. Reson. Med.*, vol. 51, no. 2, pp. 380–388, Feb. 2004.
[64] C. Ciumas *et al.*, "A phantom and animal study of temperature changes during fMRI with intracerebral depth electrodes," *Epilepsy Res.*, vol. 108, no. 1, pp. 57–65, Jan. 2014.
[65] T. M. Darcey *et al.*, "Safe use of subdermal needles for intraoperative monitoring with MRI," *Neurosurg. Focus*, vol. 40, no. 3, p. E19, Mar. 2016.
[66] R. W. Gray *et al.*, "Simple design changes to wires to substantially reduce MRI-induced heating at 1.5 T: implications for implanted leads," *Magn. Reson. Imaging*, vol. 23, no. 8, pp. 887–891, Oct. 2005.
[67] M. E. Ladd and H. H. Quick, "Reduction of resonant RF heating in intravascular catheters using coaxial chokes," *Magn. Reson. Med.*, vol. 43, no. 4, pp. 615–619, Apr. 2000.
[68] D. A. Finelli *et al.*, "MR Imaging-Related Heating of Deep Brain Stimulation Electrodes: In Vitro Study," *Am. J. Neuroradiol.*, vol. 23, no. 10, pp. 1795–1802, Nov. 2002.
[69] T. Baştuğ and S. Kuyucak, "Temperature dependence of the transport coefficients of ions from molecular dynamics simulations," Chem. Phys. Lett., vol. 408, no. 1, pp. 84–88, Jun. 2005.
[70] M. R. Singh et al., "An electrochemical engineering assessment of the operational conditions and constraints for solar-driven water-splitting systems at near-neutral pH," Energy Env. Sci, vol. 8, no. 9, pp. 2760–2767, Jun. 2015.
[71] P. Vanysek, "*Electrochemical Series*," in CRC Handbook of Chemistry and Physics, 84th ed., CRC Press, 2003, pp. 8–21, 8–31.